Digital Low-Cost FPGA Implementation of Two-Coupled and Grid-Based Network of 2D Artificial Cochlea Using the Hopf Resonator Approach

Sen Lin, Songjie Xiang, Rui Chen, Liyuan Li, Yisu Ge, Xiaoyun Gao, Mohammad Sh. Daoud, *Senior Member, IEEE*, Abdulilah Mohammad Mayet, Yanling Chu, and Yideng Huang

***Abstract*— The Cochlea, a spiral-shaped structure in the inner ear, plays a crucial role in the process of hearing by converting sound waves into electrical signals that the brain can interpret. This study introduces a cost-effective adaptation of 2D artificial Cochlea mathematical modeling using a planar approximation technique. The main novelty and contribution of our work is a method employs surface-based functions and is known as the Surface-Based Approximation Model of Cochlea (SBAMoC). By simplifying complex multiplication processes in nonlinear components, the SBAMoC reduces costs and enhances efficiency, making it suitable for FPGA implementation with minimal hardware requirements. The proposed model is evaluated in scenarios involving two-coupled oscillations and grid-based cochlear networks to better understand its performance. Through hardware synthesis on a Virtex-II board, the SBAMoC demonstrates improved efficiency and reduced computational expenses compared to the original model, achieving faster speeds and greater cost-effectiveness. In practical tests, the SBAMoC exhibits higher operational speeds and increased scalability, outperforming the original model by replicating accurate cochlear behaviors with minimal deviations. Specifically, the single SBAMoC implementation in our model achieves a speed boost of approximately 1.333 times compared to the original model (381.292 MHz vs. 286.029 MHz) and supports a greater number of fitted SBAMoCs (75 vs. 35), showcasing its superior efficiency and performance enhancements. In case of real-world applications, it can be considered for the development of more efficient and cost-effective cochlear implants, leading to improved hearing restoration solutions for individuals with hearing impairments. Also, the findings from this study could also be leveraged to enhance the design and implementation of signal processing systems in various audio and communication devices, paving the way for advanced audio processing technologies with increased efficiency and reduced hardware costs.**

***Index Terms*— Cochlea, sound waves, optimization, digital FPGA, auditory system, bio-inspired AI.**

Received 29 June 2024; revised 10 September 2024 and 2 October 2024; accepted 29 October 2024. Date of publication 15 November 2024; date of current version 30 April 2025. This work was supported in part by the Key Programs of Zhejiang Provincial Natural Science Foundation of China under Grant LZ22H130001, in part by the National Natural Science Foundation of China under Grant 82171146, in part by the Major Science and Technology Programs (The programs of opening competition mechanism to select the best candidates) of Wenzhou Science and Technology Bureau under Grant ZY2023026, and in part by the Deanship of Scientific Research at King Khalid University through the Large Group Research Project under Grant RGP2/191/45. This article was recommended by Associate Editor E. Donati. *(Corresponding authors: Yanling Chu; Yideng Huang.)*

Sen Lin and Rui Chen are with the Department of Otolaryngology, The Third Affiliated Hospital, Wenzhou Medical University, Wenzhou 325200, China (e-mail: inns@wmu.edu.cn; cr20010729@163.com).

Songjie Xiang is with the Department of Otolaryngology, The Second Affiliated Hospital and Yuying Childrens Hospital, Wenzhou Medical University, Wenzhou, Zhejiang 325000, China (e-mail: xiangsongj@hotmail.com).

Liyuan Li and Yideng Huang are with the Department of Otolaryngology, The First Affiliated Hospital, Wenzhou Medical University, Wenzhou, Zhejiang 325000, China (e-mail: liliyuanlly@hotmail.com; huangyideng@wmu.edu.cn).

Yisu Ge is with the College of Computer Science and Artificial Intelligence, Wenzhou University, Wenzhou 325100, China (e-mail: ysg@wzu.edu.cn).

Xiaoyun Gao is with the Department of Digital Media Technology, Hangzhou Dianzi University, Hangzhou 310018, China (e-mail: 19120505025@stumail.sdut.edu.cn).

Mohammad Sh. Daoud is with the College of Engineering, Al Ain University, Abu Dhabi, United Arab Emirates (e-mail: mohammad.daoud@aau.ac.ae).

Abdulilah Mohammad Mayet is with the Electrical Engineering Department, College of Engineering, King Khalid University, Abha 61421, Saudi Arabia (e-mail: amayet@kku.edu.sa).

Yanling Chu is with the Department of Otolaryngology, The Quzhou Affiliated Hospital, Wenzhou Medical University, Quzhou People's Hospital, Quzhou, Zhejiang 324000, China (e-mail: chuyanling1116@outlook.com).

Digital Object Identifier 10.1109/TCSI.2024.3494268

I. Introduction

VITAL element of the inner ear crucial for hearing is the Cochlea [1]. This component and the inner ear are closely intertwined systems that collaborate to support both hearing and balance functions [2].

As sound waves pass through the ear canal, causing the eardrum to vibrate, these vibrations travel through the middle ear bones to the oval window, creating pressure waves within the liquid-filled cochlea [3]. The Basilar Membrane (BM), which divides the cochlear duct into two sections, plays a critical function [4], [5]. Positioned on the BM, the organ of Corti houses sensory hair cells essential for converting mechanical vibrations into electrical signals. The basilar membrane is finely tuned to respond more keenly to specific frequencies along its length, with higher frequencies stimulating the cochlea's base and lower frequencies the apex [6],

[7]. The electrical signals generated within the hair cells travel through the auditory nerve fibers to the brainstem's auditory processing centers and the auditory cortex in the brain [8], [9], [10].

In case of various methods of Cochlea, one approach detailed in [11] showcases a 2-D model that demonstrates an active nonlinear Cochlea using digital hardware. Additionally, an analog VLSI implementation of the inner hair cell was outlined in [12]. Furthermore, [13] introduces an ergodic cellular automaton Cochlear model, while a hardware-efficient Cochlea model based on asynchronous cellular automaton dynamics is introduced in [14]. When focusing on the Inner Hair Cell (IHC), a real-time application proposed the Auditory Nerve Model (ANM) [15], while a digital electronic Cochlea implementation is discussed in [16]. Lastly, a Hopf resonator for a 2-D artificial Cochlea is developed and implemented in an FPGA-based scenario as described in [17].

Organic organs' mathematical models can be brought to life using two primary approaches: analog implementation and digital realization. Analog implementation constructs a neural structure mimicking mathematical models by utilizing CMOS components. While this method boosts processing speeds, it may face challenges regarding development time. Conversely, digital realization of neuronal models demands considerable silicon investment and could lead to increased power consumption. Digital implementation offers advantages such as adaptability, streamlined timing processes, and efficient power management. Leveraging programmable devices like Field-Programmable Gate Arrays (FPGAs) can offer a swift and tailored solution in this context [18], [19], [20], [21]. When employing FPGAs to manifest various organ models in hardware, a digital strategy is preferred for several reasons. Primarily, as different models possess distinct biological parameters demanding circuit design flexibility, a digital approach proves more suitable, especially when parameters deviate from those in analog designs. Secondly, digital hardware provides straightforward features and reliable implementation [22], [23], [24], [25], [26].

This research outlines a straightforward method for implementing 2D Cochlea modeling using the Hopf resonator system. The similarity between a Hopf resonator and a 2-D artificial Cochlea lies in their shared ability to display resonance phenomena and intricate nonlinear dynamics. Both systems exhibit oscillatory behavior and can be utilized to model wave-like processes or signal processing mechanisms. The study introduces a surface-based approach known as the Surface-Based Approximation Model of Cochlea (SBAMoC). This method employs linear functions to approximate a specific nonlinear function, termed the Digital-Surface-Based Approximation Model of Cochlea (D-SBAMoC), with high accuracy and minimal errors. The main contributions of our work can be listed as below:

- **SBAMoC:** This foundational model simplifies the traditional cochlear modeling approach by using surface-based linear approximations, making complex auditory processing more accessible for digital implementation.
- **Reduction of Computational Complexity:** The model addresses computational inefficiencies typical of traditional nonlinear models by substituting costly multipliers with optimized linear functions, significantly lowering the computational burden on hardware systems.
- **Optimization for Hardware Efficiency:** The SBAMoC enables substantial reductions in hardware resource requirements, facilitating real-time processing without sacrificing model fidelity. This is particularly relevant for embedded systems in cochlear implants. In this case, our proposed approach presents 52.44 % efficiency that is maximum value compared to original model and other similar approaches in the literatures.
- **Demonstrated FPGA Speed Enhancements:** Real-time implementation on the Virtex-II FPGA platform exhibits a performance increase of approximately 33.2 % compared to original model and at list 168.4 % compared to other similar models, achieving a clock speed of 381.292 MHz, thereby supporting a higher throughput for auditory signal processing.
- **Enhanced Scalability:** The proposed model allows for the integration of a greater number of cochlear units within a single FPGA core, expanding the model's scalability from 35 to 75 units. This scalability is crucial for more complex auditory simulations and applications.
- **Grid-Based Network Representation:** The extension of SBAMoC to a grid-based network provides a novel framework for examining synchronization dynamics across multiple cochlear units, paving the way for new insights into auditory processing and neural coupling behaviors.

The detailed explanation of the obtained results and performed procedure were given in different sections.

For portable hearing devices, the model can enhance sound processing efficiency, making it possible to create devices that are not only smaller and more lightweight but also more affordable. In other words, in communication systems, such as smartphones and other audio devices, the SBAMoC can improve the way these systems process sound. Enhanced algorithms could enable clearer voice recognition and better handling of background noise, resulting in more effective communication even in noisy environments. By addressing critical challenges in hardware design for auditory systems, this study not only showcases cutting-edge techniques but also emphasizes the relevance of our findings to the circuits and system designers, fostering a deeper understanding of integration at the circuit level.

The structure of the paper will be as follows: Section II discusses the modeling of 2D Cochlea. Section III presents the proposed SBAMoC. The validation of SBAMoC is described in Section IV. Discussions on two-coupled and grid-based networks are covered in Section V. The procedures for implementing D-SBAMoC in hardware are outlined in Section VI. Section VII presents discussion in Cochlea, and Section VIII concludes the paper.

II. Basic Cochlea Modeling

Recent studies have suggested that a model based on the Hopf equation effectively captures the core features of the cochlear response in simulations [27], [28], [29], [30],

[31]. Mathematically, the behavior of each resonator can be characterized by a sophisticated Hopf differential equation, as detailed in [17]:

$$\begin{cases} \dfrac{dx}{dt} = f_{orig}(x, y) + v_{trigger}(t) \\ \dfrac{dy}{dt} = g_{orig}(x, y) \end{cases} \tag{1}$$

where

$$\begin{cases} f_{orig}(x, y) = \mu x - x^3 + 3xy^2 - \omega_0 y \\ g_{orig}(x, y) = \mu y - 3yx^2 + y^3 + \omega_0 x \end{cases} \tag{2}$$

In the discussed equations, x represents the voltage signal from the Cochlea, while y is a recovery factor for generating x. The system is defined by two key parameters: μ, which influences the system's behavior through bifurcations, and ω_0 (set at 6 k.rad/s), the resonance frequency. The parameter μ controls oscillation patterns–positive values indicate limit cycles, zero leads to supercritical bifurcation, and negative values result in subcritical states. The external trigger $v_{trigger}(t)$ applies a force to the system. Challenges for digital implementation arise due to complex non-linear functions that require multiple multiplications, potentially slowing down the system. Given the fast processing speed of the human brain, a high-speed Cochlear system is necessary for effective interaction. Therefore, it's crucial to adapt the model for efficient hardware implementation.

III. Presenting the SBAMoC

Within the Cochlear modeling framework, there are two sluggish nonlinear terms (multipliers) that need to be converted into high-speed functions. During simulations involving the key variables of the system, it is observed that the variable x fluctuates within the range of -0.42 to 0.42, and the variable y ranges between -0.05 and 0.08.

Fig. 1 showcases mesh plots of the original nonlinear functions, $f_{orig}(x, y)$ and $g_{orig}(x, y)$, derived from the Hopf differential equations. These functions demonstrate complex behaviors that complicate digital implementation due to their reliance on multiple multiplication operations. In contrast, the plots also present the proposed linear functions, $f_{prop}(x, y)$ and $g_{prop}(x, y)$, which use linear approximations to closely mimic the originals with minimal error. The visual comparison illustrates that, while simplified, these linear functions maintain high fidelity to the original nonlinear dynamics, ensuring the cochlear model's accuracy and enhancing its viability for digital realization. Consequently, the revised SBAMoC formulation is as follows:

$$\begin{cases} \dfrac{dx}{dt} = f_{prop}(x, y) + v_{trigger}(t) \\ \dfrac{dy}{dt} = g_{prop}(x, y) \end{cases} \tag{3}$$

where

$$\begin{cases} f_{prop}(x, y) = p_1 x + p_2 y \\ g_{prop}(x, y) = p_{11} x + p_{22} y \end{cases} \tag{4}$$

Table I displays the parameters associated with these approximate equations. In order to minimize calculation inaccuracies, an optimization technique was utilized to ascertain these coefficients by examining all essential conditions and scenarios. We performed a systematic optimization involving a grid search for the parameters p_1, p_2, p_{11}, and p_{22}. Using error metrics like RMSE and MAE, we evaluated the differences between the original nonlinear functions and our approximations. The best parameters were chosen to minimize errors across various test scenarios for robust performance. Finally, we validated these optimized parameters by comparing the approximated model with the original using multiple validation metrics. As a result, integrating this approach can significantly boost the system's speed and decrease the overall circuit expenses. A detailed explanation of all aspects related to the hardware implementation approach and the essential considerations in the hardware segments will be provided.

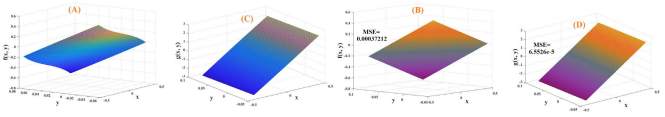

Fig. 1. The approximation method for modifying the nonlinear terms of original Cochlea. (A) Mesh plot for the original two-variable function, $f_{orig}(x, y) = \mu x - x^3 + 3xy^2 - \omega_0 y$. (B) Mesh plot for the proposed linear two-variable function, $f_{prop}(x, y) = p_1 x + p_2 y$. (C) Mesh plot for the original two-variable function, $g_{orig}(x, y) = \mu y - 3yx^2 + y^3 + \omega_0 x$. (D) Mesh plot for the proposed linear two-variable function, $g_{prop}(x, y) = p_{11} x + p_{22} y$.

TABLE I
The Optimal Parameters of Proposed Approximation Approach

$p_1 = -0.666$	$p_2 = -6$	$p_{11} = 6$	$p_{22} = -0.7934$

IV. Approval of the Proposed SBAMoC

Including timing analysis is important because it validates the efficacy of the model. It demonstrates that even after simplifying the original cochlea model by using linear approximations instead of nonlinear multipliers, the SBAMoC still yields results that are closely aligned with the original model. Moreover, phase portrait analysis adds another layer of understanding by providing visual representations that enhance our grasp of the timing analysis results. These visualizations allow for an intuitive comparison between the SBAMoC and the original model, focusing on stability and responses to different stimuli.

A. Timing Analysis

It's crucial to evaluate the calculation inaccuracies using a range of criteria [32], [33], [34], [35], [36], [37], [38], and in this instance, we utilize four appropriate error criteria:

$$\textbf{RMSE} = \sqrt{\frac{\sum_{i=1}^{n} (x_{SBAMoC} - x_{Cochlea})^2}{n}} \tag{5}$$

$$\textbf{NRMSE\%} = \frac{100}{x_{max} - x_{min}} \sqrt{\frac{\sum_{i=1}^{n} (x_{SBAMoC_i} - x_{Cochlea_i})^2}{n}} \tag{6}$$

$$\textbf{MAE} = \frac{1}{n} \sum_{i=1}^{n} |x_{SBAMoC} - x_{Cochlea.}| \tag{7}$$

$$\textbf{Corr}\% = \frac{cov(x_{Cochlea}, x_{SBAMoC})}{\sigma_{Cochlea}.\sigma_{SBAMoC}} \tag{8}$$

Table II displays the error values for each tone mode of stimulation in both the original and proposed models. The average values for different measures are: **RMSE** $= \mathbf{1.3239e-04}$, **NRMSE** $= \mathbf{0.0568}\%$, **MAE** $= \mathbf{0.0023}$, and **Corr** $= \mathbf{99.84}\%$. Furthermore, by employing different ET signals, x-based signals can be generated, as shown in Fig. 2. It is clear that the proposed model can accurately replicate the original Cochlea signaling. We will incorporate additional external trigger signals and test different types of stimuli, such as single and multi-tone signals and also with different amplitude. As can be seen in Table II (second part), different conditions based on different parameters $A1$, $W1$, $A2$, and $W2$ are considered to validate our proposed SBAMoC modeling. In this table, the Trig(A1, W1, A2, W2) = A1sin(W1πt) + A2cos(W2πt).

TABLE II

ERROR VALUES FOR DIFFERENT METRICS BASED ON DIFFERENT EXTERNAL TRIGGER (ET) AND TRIG SIGNAL

ET	RMSE	NRMSE %	MAE	Corr%
2-single tone	$5.5635e-06$	0.0083	0.0026	99.71
2-two tone	$5.3522e-07$	0.0010	0.0027	99.51
6-single tone	$8.6564e-06$	0.0043	0.0023	99.97
6-two tone	$1.2710e-04$	0.0804	0.0036	99.86
10-single tone	$1.1324e-05$	0.0034	0.0014	99.99
10-two tone	$6.4116e-04$	0.2435	0.0011	100
Mean	$\mathbf{1.3239e-04}$	**0.0568**	**0.0023**	**99.84**
Trig	**RMSE**	**NRMSE %**	**MAE**	**Corr%**
(1,10,2,20)	$5.4204e-06$	0.0163	$8.1131e-04$	99.85
(3,30,5,30)	$8.7599e-06$	0.0190	$9.4622e-04$	99.88
(4,40,7,50)	$1.0050e-05$	0.0233	0.0011	99.82
(5,60,8,60)	$9.3860e-06$	0.0225	$9.8786e-04$	99.84
(7,60,9,70)	$8.7915e-06$	0.0184	0.0012	99.82
(8,70,8,90)	$9.7159e-06$	0.0225	0.0010	99.84

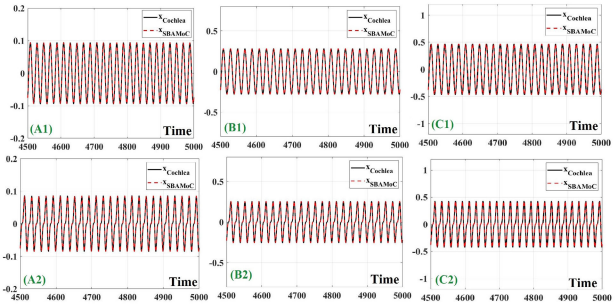

Fig. 2. Different x signals based on applying the ET = Ksin(W$_1\pi$t) + Kcos(W$_2\pi$t) to the dynamical system. (A1)-(A2): x signals for original and proposed models with ET = 2sin(10πt) + 2cos(10πt) and ET = 2sin(10πt) + 2cos(20πt), respectively. (B1)-(B2): x signals for original and proposed models with ET = 6sin(10πt) + 6cos(10πt) and ET = 6sin(10πt) + 6cos(20πt), respectively. (C1)-(C2): x signals for original and proposed models with ET = 10sin(10πt) + 10cos(10πt) and ET = 10sin(10πt) + 10cos(20πt), respectively.

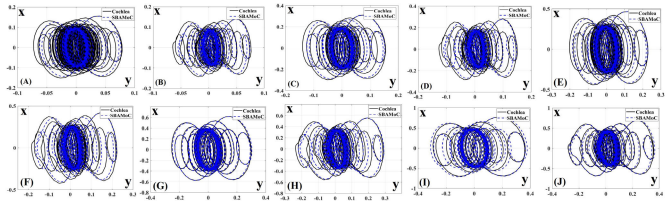

Fig. 3. Different phase portraits based on applying the ET = Ksin(W$_1\pi$t) + Kcos(W$_2\pi$t) to the dynamical system. (A): Phase portraits with ET = 2sin(10πt) + 2cos(10πt). (B): Phase portraits with ET = 2sin(10πt) + 2cos(20πt). (C): Phase portraits with ET = 4sin(10πt) + 4cos(10πt). (D): Phase portraits with ET = 4sin(10πt) + 4cos(20πt). (E): Phase portraits with ET = 6sin(10πt) + 6cos(10πt). (F): Phase portraits with ET = 6sin(10πt) + 6cos(20πt). (G): Phase portraits with ET = 8sin(10πt) + 8cos(10πt). (H): Phase portraits with ET = 8sin(10πt) + 8cos(20πt). (I): Phase portraits with ET = 10sin(10πt) + 10cos(10πt). (J): Phase portraits with ET = 10sin(10πt) + 10cos(20πt).

B. Phase Portraits Matching

Phase portraits are made up of curves that represent the system's state evolution, indicating how the system's variables change with respect to each other. Phase portraits provide insights into the system's stability, equilibrium points, and overall behavior without explicitly solving the differential equations governing the system. As can be seen in Fig. 3, the 2D phase portraits are considered for different ET. As can be seen, the proposed SBAMoC can follows the original Cochlea in case phase portrait patterns.

V. TWO-COUPLED AND GRID-BASED NETWORK OF SBAMOC

To examine the behaviors of the suggested coupling model, we implement it in a specific scenario. In this section, we analyze a pair of interconnected grid-based network oscillators described by the Hopf system. The grid-based network of cochlear models allows for a deeper analysis of how multiple cochlea units interact, mimicking the biological cochlea's sound processing. This networking is especially important for advancing cochlear implants, helping to explore how artificial cochlea units can collaborate to improve hearing restoration for those with hearing impairments.

A. Two-Coupled SBAMoC

The behavior of the two-coupled oscillators is fundamentally based on the dynamics described by the Hopf bifurcation. The Hopf equation characterizes a system undergoing a bifurcation, where a stable fixed point transitions to a limit cycle, resulting in oscillatory behaviors. This is particularly relevant when modeling cochlear dynamics, as the oscillatory nature of hair cell activity in the cochlea can be effectively captured through such equations. The standard form of the Hopf oscillation (based on our SBAMoC modeling) can be typified based on equations (3) and (4).

Specifically, in our equations for the two-coupled system, we introduce coupling terms (represented by G) which embody the interaction present in a biological cochlea as one hair cell influences the neighboring cells. In case of coupling behaviors of Hopf resonator and Cochlea, we can consider two-coupled SBAMoC structure as below formulations:

$$\begin{cases} \dfrac{dx_1}{dt} = p_1 x_1 + p_2 y_1 + v_{trigger1}(t) + G(x_2 - x_1) \\ \dfrac{dy_1}{dt} = p_{11} x_1 + p_{22} y_1 + G(y_2 - y_1) \\ \dfrac{dx_2}{dt} = p_1 x_2 + p_2 y_2 + v_{trigger2}(t) + G(x_1 - x_2) \\ \dfrac{dy_2}{dt} = p_{11} x_2 + p_{22} y_2 + G(y_1 - y_2) \end{cases} \tag{9}$$

In this model, the coupling strength G significantly influences the synchronization dynamics between the coupled

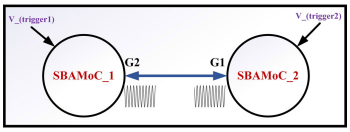

Fig. 4. Two-coupled structure of Hopf-based Cochlea with different G factors.

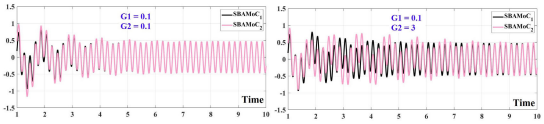

Fig. 5. Simulation of two-coupled SBAMoC oscillations with different initial values and also, different G values. The time axis is multiplied by 100.

oscillators, drawing parallels to how hair cells in the cochlea interact to enhance sound processing. In above equations, it is assumed that each oscillator is coupled linearly with the coupling strength $G > 0$. Also, as shown in Fig. 4, each of the oscillators sends a trigger signal. In fact, a two-way communication is established between both oscillators of the Cochlea. For considering the coupling behaviors of the SBAMoC, as can be depicted in Fig. 5, for different G values, the behaviors of this system is simulated. It is evident that by different values of coupling strength, the rate of synchronization between two coupled Cochlea will be reduced. In other words, these two SBAMoC can be synchronized by approximately the same coupling strength values. We consider $ET = 10sin(10\pi t) + 10cos(10\pi t)$ to test the mentioned structure.

B. Grid-Based Network

For the grid-based network, we employ a similar principle where each oscillator (node) interacts with its immediate neighbors through defined coupling strengths, similar to the two-coupled systems. The grid structure allows us to scale the model while maintaining the key features derived from the Hopf dynamics. Each node in the grid can be described by equations analogous to the coupled oscillators, reflecting how interactions occur in a two-dimensional space, leading to emergent behaviors akin to those observed in natural cochlear function.

In a grid-based network using the Hopf resonator model with a four von Neumann neighborhood in flat form, each node is connected to its four immediate neighbors (north, south, east, west) on the grid. The connectivity pattern resembles a flat grid layout, enhancing the overall resonance and coupling effects within the system [39]. This can facilitate information exchange and synchronization among nearby nodes without the need for long-range connections. Also, this can provide insights into emergent phenomena in the network. Overall, the use of a grid-based network with a four von Neumann neighborhood in a Hopf resonator model offers a balance between simplicity, local interaction, and robustness, making it a suitable choice for studying synchronization and collective dynamics in spatially structured networks. The initial configuration consists of a two-dimensional network featuring a von Neumann neighborhood arrangement illustrated in Fig. 6. In this setup, every oscillator is linked to four neighboring oscillators positioned in the cardinal directions (up, down, left, and right). To establish a mild connection between the oscillators, we make use of the state variables, denoted as x and y, of the adjacent nodes. For the jth oscillator, the following expression holds:

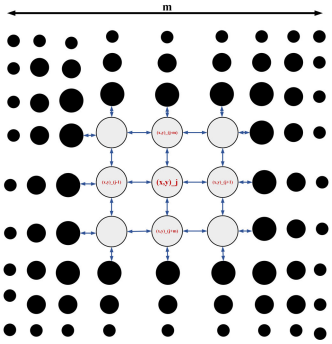

Fig. 6. Four von Neumann neighborhood network with four neighborhood oscillator connections (SBAMoC).

$$\begin{cases} \dfrac{dx_j}{dt} = p_1 x_j + p_2 y_j + G((x_{j-1} - x_j) + (x_{j+1} - x_j) + \\ (x_{j-m} - x_j) + (x_{j+m} - x_j)) \\ \dfrac{dy_j}{dt} = p_{11} x_j + p_{22} y_j + G((y_{j-1} - y_j) + (y_{j+1} - y_j) + \\ (y_{j-m} - y_j) + (y_{j+m} - y_j)) \end{cases} \tag{10}$$

In the arrangement with m oscillators per row, it's worth mentioning that because of the planar layout of this system, edge oscillators have interactions with only two or three neighboring oscillators. For instance, the oscillator positioned in the top right corner connects with two neighboring oscillators below and to the left. To demonstrate the impact of network connections, the network was initialized with varying initial values for x, y, and G. The network's dynamics are illustrated in Fig. 7, revealing that all oscillators eventually synchronize to a unified signal with consistent phase and frequency, resulting in synchrony. This figure depicts the dynamics of a 4×4 grid-based network of SBAMoCs, specifically illustrating the coupling behaviors of the proposed model. Each node in the grid corresponds to a separate SBAMoC unit, and the figure shows how the signals x_1 to x_{16} evolve over time as a result of the triggering inputs. The figure highlights the interactions between neighboring nodes based on different G, emphasizing the impact of coupling strength on synchronization. Notably, the figure also showcases variations in amplitude and frequency across different nodes, indicating how the grid structure influences the overall dynamical behavior of the system. It's important to highlight that in this network, an input stimulus is introduced with the form $ET = 10\sin(10\pi t) + 10\cos(10\pi t)$, specifically targeted at the initial columns of the network under consideration. Moreover, in our simulations, we have assumed that a network of 4×4 matrix of SBAMoC (proposed Cochlea) is simulated.

VI. Digital SBAMoC Implementation

In this part, we will evaluate the feasibility of putting into practice both the current and suggested Cochlea models in hardware, emphasizing performance and effectiveness in

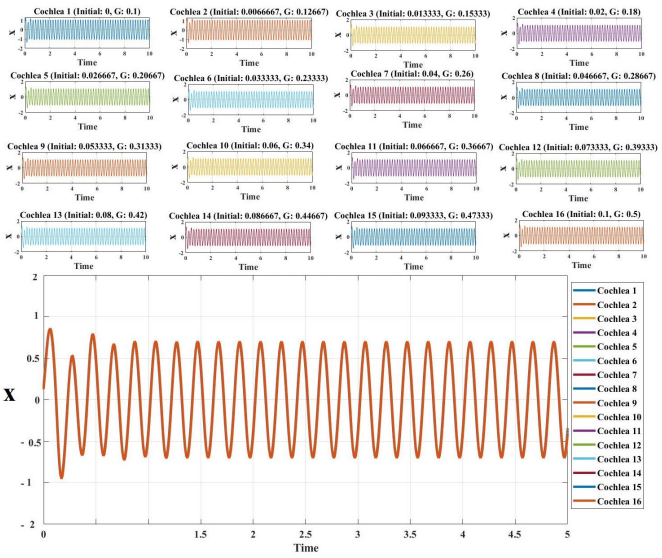

Fig. 7. x_1 to x_{16} for a 4×4 matrix of oscillators that have been coupled based on four von Neumann neighborhood using the SBAMoC.

different design processes [40]. Moreover, two linked and lattice-style networks have been constructed. Future sections will delve into executing the suggested SBAMoC in a hardware environment.

A. Discretization

The initial stage in commencing and constructing the digital rendition of the specific Cochlea model involves discretizing the equations and components of the model. To transform the Cochlea model into digital hardware, every aspect of the model must undergo digitization. Numerous techniques exist for discretizing first-order differential equations, with one basic approach being Euler's method. When implementing the Euler method, the fundamental elements of the Cochlea model are outlined as follows:

$$\begin{cases} x[n+1] = dt * [(\mu - x^2[n] + 3y^2[n])x[n] - \\ \omega_0 y[n] + v[n]] + x[n] \\ y[n+1] = dt * [(\mu - 3x^2[n] + y^2[n])y[n] + \\ \omega_0 x[n]] + y[n] \end{cases} \tag{11}$$

And for the proposed elements are given as below:

$$\begin{cases} x[n+1] = dt * [p_1 x[n] + p_2 y[n] + v[n]] + x[n] \\ y[n+1] = dt * [p_{11} x[n] + p_{22} y[n]] + y[n] \end{cases} \tag{12}$$

B. Evaluation of Required Bit-Width

In digital systems, numbers are typically represented using fixed-point or floating-point formats. Although floating-point offers greater precision, it demands more resources and can slow down circuits, making fixed-point representation more suitable for FPGA-based systems where speed and resource limitations are critical. In our model, we chose a bit-width of 21 bits, allocating 5 bits for the integer part, 15 bits for the fractional part, and 1 bit for the sign. This decision is based on the extreme values of variables, the potential for maximum shifts, and the necessity to avoid overflow, ensuring optimal performance in digital design.

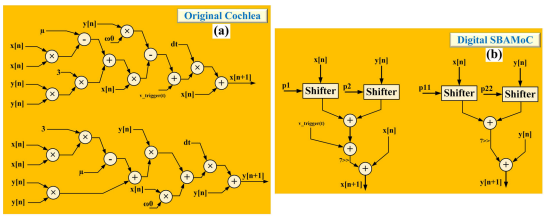

Fig. 8. (a) The original Cochlea model provides scheduling diagrams for two key variables. It is evident that the numerous multiplications in the design may decrease the system frequency and increase the hardware resource demands. (b) Digital SBAMoC circuits can be implemented using cost-effective components like shifters and adders.

C. Digital Circuits of SBAMoC

Fig. 8 illustrates the timing diagrams of two key variables for the original Cochlea and the economical digital SBAMoC. In the original Cochlea case (Fig. 8(a)), it is apparent that multiple multiplication components are necessary for implementing this initial model. The multiplication unit is identified as an expensive component that can negatively impact both the hardware cost and processing speed of the neural system. Conversely, as shown in Fig. 8 (b), the proposed SBAMoC model was developed without any multiplications. In this approach, 4 approximation parameters can be converted to digital numbers as: $p_1 = -0.666 = -(1/2 + 1/8 + 1/32 + 1/128 + 1/512)$, $p_2 = -6 = -(4 + 2)$, $p_{11} = 6 = (4 + 2)$, and $p_{22} = -0.7934 = -(1/2 + 1/4 + 1/32 + 1/128 + 1/256 + 1/2048)$. Converting multiplications to digital shifts and adders simplifies calculations in digital systems by using binary representation. Multiplying a number by 2 or its powers is achieved with left shifts, while right shifts help divide by powers of 2, making them useful for fractions and negative numbers. In the digital SBAMoC scenario, as illustrated, only shifters and adders are present in cost-effective configurations. Specifically, four predefined parameters, p_1, p_2, p_{11}, and p_{22}, are responsible for transforming the multiplications into digital shifters and adders, which are inexpensive modules compared to the elements in the original model.

D. SBAMoC Digital Realization Results

In order to validate the proposed model effectively, it is essential to showcase the results of hardware synthesis. This demonstration plays a critical role in verifying the authenticity of the model and the suggested approach. The Virtex-II Pro XC2VP30 Platform FPGA is employed for the hardware implementation of both the original and proposed models. The detailed results of the hardware synthesis for the original and proposed models can be found in Table III. In the context of hardware synthesis, the evaluation includes analyzing the quantity of slice registers (or Flip Flops, FFs), the number of slice LUTs, Available Resources (AR), Maximum Cochlea Fitted on Chip (MCFoC), and the synthesis frequency. Additionally, two key metrics, AR and MCFoC, can be explained as follows: The Available Resources (AR) metric signifies the maximum utilization percentage of the board's hardware resources (up to 100%). This can be exemplified as:

$$\text{AR} = \left(\frac{\text{Utilized Resources}}{\text{Available}}\right) \times 100\% \tag{13}$$

TABLE III
EMPLOYMENT OF XILINX VIRTEX-II AT A BASIC LEVEL AND THE RATIO OF FUNDAMENTAL COMPONENTS USED IN BUILDING THE COCHLEA MODEL

Target Model	FFs	LUTs	Frequency (MHz)	AR	MCFoC	Speed-Up	Power Consumption (mW)
Original Cochlea	560(2.04%)	781(2.85%)	286.029	2.85%	35	1	214
Proposed D-SBAMoC	342(1.25%)	364(1.32%)	381.292	1.32%	75	1.333	95
Nouri [17]	400(1.46%)	451(1.64%)	339.795	1.64%	60	1.188	NA

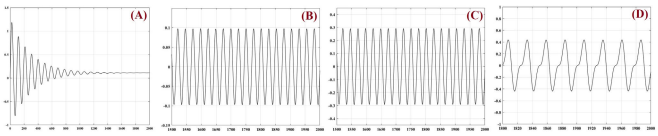

Fig. 9. Digital data of SBAMoC signaling for different ET as (A): 10 without tones. (B) 2 with single tone state. (C) 6 with single tone state. (D) 10 with two tone state.

The calculation for determining the maximum quantity of Cochleas is derived using the MCFoC metric, as illustrated in the equation below:

$$\text{MCFoC} = \frac{100}{\text{AR}} \tag{14}$$

Table III presents a comparison of Cochlea quantities between the initial and proposed models (Referenced in [17]). Our proposed model, as depicted in the table, exhibits enhanced speed (frequency) and reduced overhead costs in contrast to the original model. Notably, the parameter MCFoC plays a significant role in determining the feasible number of D-SBAMoC units on a single FPGA core. The removal of multiplier modules in our proposed model contributes to cost reduction and facilitates a swift digital design process. Conversely, the original Cochlea model, with its multiple internal multipliers, results in a slower system with higher costs due to prolonged critical paths during circuit implementation. The pivotal factors, MCFoC and frequency, validate the superior efficiency of our proposed model compared to the original design. Our model accommodates a greater number of MCFoC units (75 compared to 60) and offers a faster implementation speed (381.292 MHz compared to 339.795 MHz). Additionally, Fig. 9 demonstrates that the digital data produced by our proposed D-SBAMoC model closely aligns with the signals of the original model. It highlights how the output signals for different external stimuli (such as different amplitude tones) compare between the original model and the proposed model. Due to eliminating all multipliers and high-cost terms, the power consumption of our proposed model is less than the original model.

The SBAMoC enhances energy efficiency in devices for hearing restoration by reducing computational load, simplifying hardware architecture, and allowing greater scalability. By replacing power-hungry multipliers with simpler adders and shifters, it lowers power consumption and costs. This efficiency is particularly beneficial for portable devices like cochlear implants and hearing aids, extending battery life and usability. Overall, the SBAMoC is well-suited for mobile applications where minimizing power consumption is crucial.

We have included a comparative table (Table IV) that outlines key performance metrics such as speed, resource utilization (Flip-Flops and LUTs), and the maximum number of Cochleas that can be fitted on the FPGA. The results show significant improvements:

- Speed increased from 286.029 MHz to 381.292 MHz, which is a 33.2% improvement.
- Utilization of Flip-Flops and LUTs decreased by 38.9% and 53.4%, respectively.
- The MCFoC increased from 35 to 75, representing a 114.3% increase.

We have included bar charts (Fig. 10) that visually illustrate these performance improvements (based on two key factors: resource saving and speed), making the enhancements more apparent. The improvements can be attributed to the elimination of complex multiplication operations by using simpler linear functions, which effectively enhanced the overall speed of the digital system. The use of shifters and adders in the SBAMoC contributed to reduced circuit costs, allowing more efficient FPGA utilization.

The synthesized frequency of 381.292 MHz pertains to the overall computational capacity of our FPGA implementation, not the frequencies of the sound signals processed by the cochlea (typically 20 Hz to 20 kHz). The higher synthesized frequency enables efficient execution of complex signal processing tasks, ensuring real-time performance while allowing for flexibility in handling various input conditions. This approach incorporates power management strategies to optimize energy consumption without sacrificing performance. Although a higher clock frequency typically increases power consumption, modern FPGA designs employ power management strategies like dynamic voltage scaling and clock gating.

TABLE IV
COMPARISON OF PERFORMANCE METRICS FOR ORIGINAL MODEL AND SBAMOC

Metric	Original Model	SBAMoC	Improvement
Speed (MHz)	286.029	381.292	+33.2%
Flip-Flops Used	560	342	-38.9%
LUTs Used	781	364	-53.4%
MCFoC	35	75	+114.3%

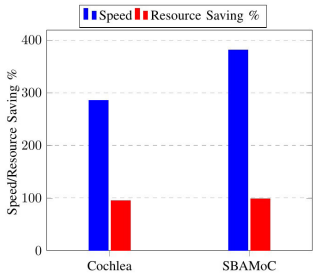

Fig. 10. Comparison between two basic factors: speed and resource saving for two original Cochlea and proposed SBAMoC models.

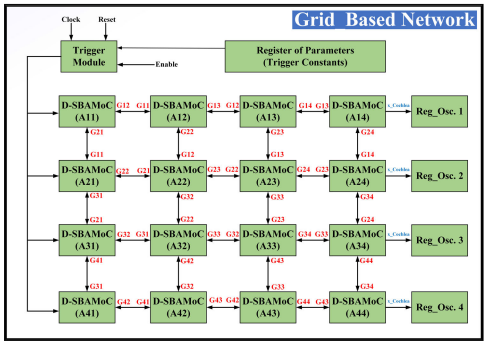

Fig. 11. An array of 4×4 grid-based network using the D-SBAMoC. Each unit connect to other 4 points one via coupling strength of G_{ij}.

TABLE V
SYNTHESIS RESULTS OF GRID-BASED D-SBAMOC

Coupling	Flip Flop	LUT	Speed	MCFoC
2-Coupled	648(2.36%)	685(2.5%)	380.164 MHz	80
16-Multiplexed	1421(5.2%)	1753(6.4%)	377.287 MHz	250

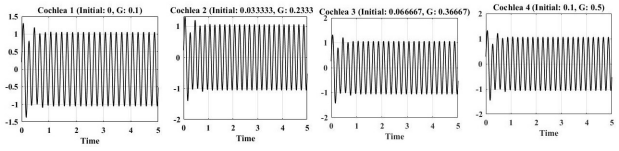

Fig. 12. Outputs of D-SBAMoC in grid states. Time is multplied by 1000.

E. Grid-Based D-SBAMoC Realization

The intended network is shown in Fig. 11. As you can see, this is a 4×4 array, each of its units is connected to four adjacent units. To realize this network, we first apply a trigger signal to the first column of the arrays so that the oscillators start to oscillate. Then, based on the coupling coefficient between each of the units (which interact with each other), oscillatory signals are emitted.

By employing resource sharing and time multiplexing techniques, the efficiency and utilization of available resources can be significantly improved. This can prevent wastage of resources and improve scalability. Different processes or users are then allocated these time slots sequentially. Time multiplexing allows multiple users to share the same resource by interleaving their access to it. Thus, by combining these two techniques, systems can optimize resource utilization, reduce costs, and improve overall performance. Table V shows the realization of grid D-SBAMoC using the mentioned techniques. Also, the outputs of oscillation signallings are depicted in Fig. 12 for 4 Cochlea output units of grid network. Fig. 12 demonstrates that the digital data produced by our proposed D-SBAMoC model in network-based state (based on Fig. 11). Using multiple D-SBAMoC units on a single FPGA boosts applications like cochlear implants and hearing aids by enhancing frequency simulation and reducing the realization costs (increasing number of coupled Cochlea), improving adaptability, and enabling real-time processing. It also aids auditory research and supports complex auditory modeling. Overall, it enhances flexibility and scalability in auditory systems.

VII. DISCUSSION

A. Limitations of the SBAMoC

One major limitation lies in its reliance on linear approximations, which may not fully capture the complex nonlinear dynamics inherent in biological cochlear function. This simplification could lead to some levels of errors. Moreover, the accuracy of the SBAMoC is contingent upon the optimization of the coefficients p_1, p_2, p_{11}, and p_{22} and can be sensitive to the tuning of these parameters.

B. Challenges in Large-Scale Implementation

As system scale increases, the complexity of interconnections can lead to higher latency and power consumption during synchronization. Effectively managing the coupling strengths G across a large grid is crucial for stability, but varying conditions can complicate achieving uniform performance. Integrating multiple SBAMoCs into a compact FPGA architecture requires careful resource allocation and signal routing to avoid congestion, particularly in resource-limited environments.

C. Types of FPGAs and Their Considerations

Different FPGA platforms, such as Xilinx Zynq or Altera Cyclone series, come with varying capabilities, including logic density, speed, and power efficiency. When selecting an FPGA for implementing SBAMoC, factors such as available resources (LUTs, DSPs), speed specifications, and I/O capabilities must be considered. Furthermore, newer FPGAs may offer enhanced features such as integrated processors or specific DSP blocks that could optimize the implementation of complex algorithms. The Virtex-2 FPGA board meets our current project needs effectively due to its performance, cost-effectiveness, and available resources. However, we are excited about exploring modern FPGAs in the future for their enhanced capabilities, lower power consumption, and compatibility with advanced technologies.

D. Comparison With Cochlear Models

Table VI compares various digital cochlea models, highlighting the Surface-Based Approximation Model of Cochlea (SBAMoC) alongside established models. It details the FPGA architecture used, the count of flip-flops (FFs) and look-up tables (LUTs) for design efficiency, and the operational frequency in MHz to indicate processing speed and performance. Finally, efficiency is calculated using the formula:

$$\text{Efficiency} = \left(\frac{\text{Frequency}}{\text{FFs} + \text{LUTs}}\right) \times 100\% \tag{15}$$

The SBAMoC model offers notable advantages, including low resource usage with only 342 flip-flops and 364 LUTs, leading to a high operational frequency of 381.292 MHz and an efficiency of 52.44%. However, it also has drawbacks, such as relying on linear approximations that may miss complex biological behaviors, affecting model accuracy. Additionally, its performance can be sensitive to coefficient tuning, requiring careful adjustments in different applications.

TABLE VI
COMPARISON OF DIGITAL COCHLEA MODELS WITH VARIOUS APPROACHES

Digital Cochlea Model	Base Approach	FPGA Board	FFs	LUTs	Frequency (MHz)	Efficiency (%)
D-SBAMoC	Hopf Modeling	Virtex-2	342	364	381.292	52.44%
Reference [11]	Hopf Modeling	Artix-7	133	1621	20	1.22%
Reference [41]	Asynchronous Modeling	Artix-7	76	792	100	12.47%
Reference [42]	Spiral Ganglion Cell Modeling	Zynq	820	2625	100	3.66%
Reference [13]	Cellular Automaton Modeling	Artix-7	126	628	100	15.75%
Reference [43]	Hopf Modeling	Artix-7	161	6666	100	1.49%
Reference [44]	Hopf Modeling	Artix-7	216	3713	100	2.61%
Reference [45]	CAR Modeling	Virtex-6	113760	136957	142	0.10%

TABLE VII
A DETAILED COST-BENEFIT ANALYSIS CONSIDERING HARDWARE, DEVELOPMENT, AND MAINTENANCE COSTS OVER THE DEVICE'S LIFECYCLE

Cost Category	Description	Cost ($)
Hardware Costs		
	FPGA Cost	130
	Additional Components	20
	Development Board	20
	Cooling Costs	10
	Power Supply Costs	50
	Total Hardware Costs	**230**
Development Costs		
	Labor Costs (Hourly Rate * Hours Worked)	10/hour * 30 hours = 300
	Tools and Software Costs	20
	Total Development Costs	**320**
Maintenance Costs		
	Software Update Costs	15
	Repair/Replacement Costs (over 5 years)	50/year * 5 = 250
	Total Maintenance Costs	**265**
Total Costs	**Total Hardware + Development + Maintenance**	**815**

E. Cost-Benefit Analysis

The cost-benefit for the SBAMoC implementation is detailed in Table VII. The hardware costs total $230, which includes the FPGA, additional components, and the development board. The development phase incurs a total cost of $320, primarily driven by labor expenses and necessary tools and software. Lastly, maintenance costs over a five-year period amount to $265, including software updates and potential repair or replacement costs. Overall, the total estimated cost for the project is $815, providing a comprehensive overview of the financial requirements for the successful implementation of the Cochlea model.

F. Future Implementations and Clinical Validation

For prototype development, we aim to transition from FPGA to ASIC designs for scalability and integrate SBAMoC with auditory sensors for real-time processing. Clinical validation steps include performing pre-clinical tests on biophysical models and conducting pilot clinical trials using randomized control designs. User feedback will be collected regarding comfort and usability, allowing us to iteratively refine the model and design based on insights. We will also explore the adaptation of the model to various hardware platforms, investigating performance across different systems and developing simulations for adaptability testing. Finally, we plan to collaborate with experts in relevant fields to enhance our implementation efforts. This plan aims to rigorously validate our SBAMoC model and explore its application across multiple platforms.

VIII. CONCLUSION

This research focuses on the implementation of the 2D artificial Cochlea model. The timing analysis reveals a similarity level of approximately 99.84%. Moreover, the RMSE values were found to be around 10^{-4}. A digital hardware design was created for the suggested model, and a comparison was conducted with the original approach in terms of resource utilization and accuracy assessment (evaluating AR and MCFoC parameters). Subsequently, the proposed digital system was synthesized on the Xilinx Virtex-II FPGA board, achieving a speed of 381.292 MHz for the proposed model. Examination of hardware expenses indicates that the proposed model consumes merely 1.32% of FPGA hardware resources (AR), allowing for the deployment of 75 D-SBAMoC units on a single FPGA core (MCFoC). The hardware outcomes showcase the effectiveness of the proposed model in speed, cost, and the maximum number of D-SBAMoCs implemented on a single FPGA core compared to the original model. Furthermore, the proposed model underwent testing in a grid-based network of 4×4 arrays. The network was also constructed and synthesized, demonstrating MCFoC of 250 and a frequency of 377.287 MHz.

REFERENCES

[1] E. C. Driver and M. W. Kelley, "Development of the cochlea," *Development*, vol. 147, no. 12, Jun. 2020, Art. no. dev162263.

[2] M. G. Carpenter and J. L. Campos, "The effects of hearing loss on balance: A critical review," *Ear Hearing*, vol. 41, pp. 107S–119S, Nov. 2020.

[3] F.-G. Zeng, *Compression and Cochlear Implants*. Cham, Switzerland: Springer, 2004.

[4] T. J. Hamilton, J. Tapson, C. Jin, and A. van Schaik, "Analogue VLSI implementations of two dimensional, nonlinear, active cochlea models," in *Proc. IEEE Biomed. Circuits Syst. Conf.*, Nov. 2008, pp. 153–156.

[5] M. P. Leong, C. T. Jin, and P. H. W. Leong, "An FPGA-based electronic cochlea," *EURASIP J. Adv. Signal Process.*, vol. 2003, no. 7, pp. 629–638, Jun. 2003.

[6] S. Wang, T. J. Koickal, A. Hamilton, R. Cheung, and L. S. Smith, "A biorealistic analog CMOS cochlea filter with high tunability and ultra-steep roll-off," *IEEE Trans. Biomed. Circuits Syst.*, vol. 9, no. 3, pp. 297–311, Jun. 2015, doi: 10.1109/TBCAS.2014.2328321.

[7] T. Gold and J. Gray, "Hearing. II. The physical basis of the action of the cochlea," *Proc. Roy. Soc. B, Biol. Sci.*, vol. 135, no. 881, pp. 492–498, Dec. 1948.

[8] R. F. Lyon and C. Mead, "An analog electronic cochlea," *IEEE Trans. Acoust., Speech, Signal Process.*, vol. 36, no. 7, pp. 1119–1134, Jul. 1988.

[9] Y. Choe, M. O. Magnasco, and A. J. Hudspeth, "A model for amplification of hair-bundle motion by cyclical binding of Ca^{2+} to mechanoelectrical-transduction channels," *Proc. Nat. Acad. Sci.*, vol. 95, no. 26, pp. 15321–15326, 1998.

[10] W. E. Brownell, C. R. Bader, D. Bertrand, and Y. de Ribaupierre, "Evoked mechanical responses of isolated cochlear outer hair cells," *Science*, vol. 227, no. 4683, pp. 194–196, Jan. 1985.

[11] M. A. Alsakkal and J. H. B. Wijekoon, "An active Hopf-based digital hardware cochlea implementation," in *Proc. IEEE Symp. Ser. Comput. Intell. (SSCI)*, Dec. 2022, pp. 664–671, doi: 10.1109/SSCI51031.2022.10022303.

[12] D. S. Freedman, H. I. Cohen, S. Deligeorges, C. Karl, and A. E. Hubbard, "An analog VLSI implementation of the inner hair cell and auditory nerve using a dual AGC model," *IEEE Trans. Biomed. Circuits Syst.*, vol. 8, no. 2, pp. 240–256, Apr. 2014.

[13] I. Kubota, K. Takeda, and H. Torikai, "A novel ergodic cellular automaton cochlear model: Reproduction of nonlinear sound processing functions of mammalian cochlea and efficient hardware implementation," in *Proc. Int. Joint Conf. Neural Netw. (IJCNN)*, Jul. 2022, pp. 1–8.

[14] I. Kubota and H. Torikai, "A novel hardware-efficient cochlea model based on asynchronous cellular automaton dynamics: Two-tone suppression and FPGA implementation," in *Proc. 17th Int. Workshop Cellular Nanosc. Netw. their Appl. (CNNA)*, Sep. 2021, pp. 1–4.

[15] R. James, J. Garside, L. A. Plana, A. Rowley, and S. B. Furber, "Parallel distribution of an inner hair cell and auditory nerve model for real-time application," *IEEE Trans. Biomed. Circuits Syst.*, vol. 12, no. 5, pp. 1018–1026, Oct. 2018.

[16] A. Paul and K. P. Menon, "Digital implementation of hyperbolic calculation unit for electronic cochlea on FPGA," in *Proc. 2nd IEEE Int. Conf. Recent Trends Electron., Inf. Commun. Technol. (RTEICT)*, May 2017, pp. 1322–1325.

[17] M. Nouri, A. Ahmadi, S. Alirezaee, G. Karimi, M. Ahmadi, and D. Abbott, "A Hopf resonator for 2-D artificial cochlea: Piecewise linear model and digital implementation," *IEEE Trans. Circuits Syst. I, Reg. Papers*, vol. 62, no. 4, pp. 1117–1125, Apr. 2015.

[18] Y. Ge et al., "High-machting and low-cost realization of the FHN neuron model on reconfigurable FPGA board," in *Proc. IEEE Trans. Biomed. Circuits Syst.*, Apr. 2024, vol. 18, no. 2, p. 451, doi: 10.1109/TBCAS.2023.3337335.

[19] G. Zhang et al., "Investigation on the Wilson neuronal model: Optimized approximation and digital multiplierless implementation," *IEEE Trans. Biomed. Circuits Syst.*, vol. 16, no. 6, pp. 1181–1190, Dec. 2022.

[20] G. Zhang et al., "Efficient implementation of spontaneous calcium oscillations in the central nervous system on reconfigurable digital boards," *IEEE Trans. Circuits Syst. I, Reg. Papers*, vol. 70, no. 6, pp. 2478–2486, Jun. 2023.

[21] Y. Chen et al., "Digital approach in case of FPGA realization of quartic neuron model (QNM) using cost-effective mathematical modifications," *IEEE Trans. Circuits Syst. I, Reg. Papers*, early access, May 22, 2024, doi: 10.1109/TCSI.2024.3400399.

[22] S. Haghiri, A. Zahedi, A. Naderi, and A. Ahmadi, "Multiplierless implementation of noisy Izhikevich neuron with low-cost digital design," *IEEE Trans. Biomed. Circuits Syst.*, vol. 12, no. 6, pp. 1422–1430, Dec. 2018, doi: 10.1109/TBCAS.2018.2868746.

[23] M. Nouri, M. Hayati, T. S. Gotarredona, and D. Abbott, "A digital neuromorphic realization of the 2-D Wilson neuron model," *IEEE Trans. Circuits Syst. II, Express Briefs*, vol. 66, no. 1, pp. 136–140, Nov. 2019.

[24] E. Jokar, H. Abolfathi, and A. Ahmadi, "A novel nonlinear function evaluation approach for efficient FPGA mapping of neuron and synaptic plasticity models," *IEEE Trans. Biomed. Circuits Syst.*, vol. 13, no. 2, pp. 454–469, Apr. 2019, doi: 10.1109/TBCAS.2019.2900943.

[25] S. Majidifar, M. Hayati, M. R. Malekshahi, and D. Abbott, "Low cost digital implementation of hybrid FitzHugh Nagumo–Morris lecar neuron model considering electromagnetic flux coupling," *IEEE Trans. Biomed. Circuits Syst.*, vol. 16, no. 6, pp. 1366–1374, Dec. 2022.

[26] S. Haghiri and A. Ahmadi, "A novel digital realization of AdEx neuron model," *IEEE Trans. Circuits Syst. II, Express Briefs*, vol. 67, no. 8, pp. 1444–1448, Aug. 2020.

[27] R. Fettiplace, "Hair cell transduction, tuning, and synaptic transmission in the mammalian cochlea," *Comprehensive Physiol.*, vol. 7, no. 4, pp. 1197–1227, 2017.

[28] A. Altoe and C. A. Shera, "The cochlear ear horn: Geometric origin of tonotopic variations in auditory signal processing," *IEEE Trans. Circuits Syst. II*, vol. 67, no. 8, pp. 1444–1448, Aug. 2020.

[29] A. Kern and R. Stoop, "Essential role of couplings between hearing nonlinearities," *Phys. Rev. Lett.*, vol. 91, no. 12, 2003, Art. no. 128101.

[30] V. M. Eguiluz, M. Ospeck, Y. Choe, A. J. Hudspeth, and M. O. Magnasco, "Essential nonlinearities in hearing," *Phys. Rev. Lett.*, vol. 84, no. 22, p. 5232, 2000.

[31] S. Camalet, T. Duke, F. Julicher, and J. Prost, "Auditory sensitivity provided by self-tuned critical oscillations of hair cells," *Proc. Nat. Acad. Sci. USA*, vol. 97, no. 7, pp. 3183–3188, 2000.

[32] S. Haghiri, A. Naderi, B. Ghanbari, and A. Ahmadi, "High speed and low digital resources implementation of Hodgkin-Huxley neuronal model using base-2 functions," *IEEE Trans. Circuits Syst. I, Reg. Papers*, vol. 68, no. 1, pp. 275–287, Jan. 2021.

[33] S. Haghiri, S. I. Yahya, A. Rezaei, and A. Ahmadi, "Multiplierless implementation of Fitz-Hugh Nagumo (FHN) modeling using CORDIC approach," *IEEE Trans. Emerg. Topics Comput. Intell.*, vol. 8, no. 1, pp. 279–287, Feb. 2024.

[34] S. Haghiri, S. I. Yahya, A. Rezaei, and A. Ahmadi, "Multiplierless low-cost implementation of Hindmarsh–Rose neuron model in case of large-scale realization," *Int. J. Circuit Theory Appl.*, vol. 51, no. 6, pp. 2966–2980, Jun. 2023.

[35] M. Heidarpur, A. Ahmadi, M. Ahmadi, and M. R. Azghadi, "CORDIC-SNN: On-FPGA STDP learning with Izhikevich neurons," *IEEE Trans. Circuits Syst. I, Reg. Papers*, vol. 66, no. 7, pp. 2651–2661, Jul. 2019, doi: 10.1109/TCSI.2019.2899356.

[36] M. Heidarpur, P. Khosravifar, A. Ahmadi, and M. Ahmadi, "CORDIC-astrocyte: Tripartite glutamate-IP3-Ca^{2+} interaction dynamics on FPGA," *IEEE Trans. Biomed. Circuits Syst.*, vol. 14, no. 1, pp. 36–47, Feb. 2020.

[37] E. Jokar, H. Abolfathi, A. Ahmadi, and M. Ahmadi, "An efficient uniform-segmented neuron model for large-scale neuromorphic circuit design: Simulation and FPGA synthesis results," *IEEE Trans. Circuits Syst. I, Reg. Papers*, vol. 66, no. 6, pp. 2336–2349, Jun. 2019.

[38] S. Gomar and A. Ahmadi, "Digital multiplierless implementation of biological adaptive-exponential neuron model," *IEEE Trans. Circuits Syst. I, Reg. Papers*, vol. 61, no. 4, pp. 1206–1219, Apr. 2014.

[39] H. Soleimani, M. Bavandpour, A. Ahmadi, and D. Abbott, "Digital implementation of a biological astrocyte model and its application," *IEEE Trans. Emerg. Topics Comput. Intell.*, vol. 26, no. 1, pp. 127–139, Jan. 2015.

[40] S. Gomar and M. Ahmadi, "Digital hardware implementation of Gaussian Wilson–Cowan neocortex model," *IEEE Trans. Emerg. Topics Comput. Intell.*, vol. 3, no. 1, pp. 24–35, Feb. 2019.

[41] K. Takeda and H. Torikai, "A novel hardware-efficient cochlea model based on asynchronous cellular automaton dynamics: Theoretical analysis and FPGA implementation," *IEEE Trans. Circuits Syst. II, Exp. Briefs*, vol. 64, no. 9, pp. 1107–1111, Sep. 2017.

[42] M. Izawa and H. Torikai, "Nonlinear responses of an asynchronous cellular automaton model of spiral ganglion cell," in *Proc. Int. Joint Conf. Neural Netw. (IJCNN)*, Jul. 2014, pp. 2483–2490, doi: 10.1109/IJCNN.2014.6889594.

[43] A. Kern and R. Stoop, "Essential role of couplings between hearing nonlinearities," in *Proc. Int. Joint Conf. Neural Netw. (IJCNN)*, 2003, pp. 1–4, doi: 10.1103/PhysRevLett.91.128101.

[44] K. Takeda and H. Torikai, "Two-tone distortion products in hardware-efficient cochlea model based on asynchronous cellular automaton oscillator," *IEICE Electron. Express*, vol. 18, no. 18, 2021, Art. no. 20210310, doi: 10.1587/elex.18.20210310.

[45] C. S. Thakur, T. J. Hamilton, J. Tapson, A. van Schaik, and R. F. Lyon, "FPGA implementation of the CAR model of the cochlea," in *Proc. IEEE Int. Symp. Circuits Syst. (ISCAS)*, Jun. 2014, pp. 1853–1856, doi: 10.1109/ISCAS.2014.6865519.

Sen Lin received the master's degree from Wenzhou Medical University in 2011. He is currently the Chief Physician and the Subject Leader of the Third Affiliated Hospital, Wenzhou Medical University. He is mainly engaged in basic and clinical research on inner ear medication and cochlear implants.

Songjie Xiang received the B.M. and M.M. degrees from Wenzhou Medical University, Wenzhou, China, in 1995 and 2007, respectively. Her main research interests include clinical and basic research of middle ear and inner ear diseases.

Rui Chen received the bachelor's degree in medicine from the Wannan Medical College, Wuhu, China, in 2024. She is currently pursuing the master's degree with Wenzhou Medical University. Her current research interests include nanomedicine delivery to the inner ear and cochlear implants.

Liyuan Li received the bachelor's degree in medicine from Hangzhou City University, Hangzhou, China, in 2016. He is currently pursuing the master's degree with Wenzhou Medical University. His research interests include nerve regeneration and brain plasticity.

Yisu Ge received the B.S. degree in computer science engineering from Zhejiang University of Technology, Hangzhou, China, in 2016, and the Ph.D. degree in control science and engineering from Zhejiang University, Hangzhou, Zhejiang, China, in 2021. Since 2021, he has been a Lecturer with Wenzhou University. His research interests include visual object tracking, object detection, and medical image segmentation.

Xiaoyun Gao received the bachelor's degree from Shandong University of Technology. She is currently pursuing the master's degree in digital media technology with Hangzhou Dianzi University, with a focus on intelligent media computing.

Mohammad Sh. Daoud (Senior Member, IEEE) received the Ph.D. degree in computer science from De Montfort University, U.K. He is currently an Associate Professor with the College of Engineering, Al Ain University, United Arab Emirates. His research interests include artificial intelligence, swarm systems, secured systems and networks, and smart applications.

Abdulilah Mohammad Mayet received the M.Sc. and Ph.D. degrees from the King Abdullah University of Science and Technology (KAUST). He is currently a 2030 Leader at the MiSK Foundation and an Assistant Professor at King Khalid University, teaching courses in nanofabrication and FPGA for AI. He is also the Director of the Engineering College Research Center and a Consultant at the Artificial Intelligence Center (AIC). He has a research collaboration with the University of California, Irvine, and Cornell University.

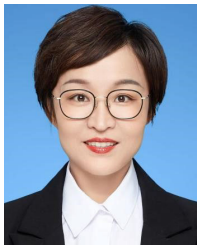

Yanling Chu received the master's and Ph.D. degrees from China Medical University, Taiwan, in 2011 and 2016, respectively. Her main research interests include basic research on allergic rhinitis and hard of hearing.

Yideng Huang received the Ph.D. degree in clinical medicine (otolaryngology) from Second Military Medical University, China, in 2004. He is currently with the Otolaryngology Department, The First Affiliated Hospital, Wenzhou Medical University. His research interests include pathogenesis and drug screening of genetic and sensorineural hard of hearing.